Structure of a Fructose-1,6-bis(phosphate) Aldolase Liganded to Its Natural Substrate in a Cleavage-Defective Mutant at 2.3 Å[†,‡]

Kyung H. Choi,[§,||] Andrew S. Mazurkie,[§] Aaron J. Morris,[||,⊥] Didier Utheza,[§] Dean R. Tolan,[||] and Karen N. Allen*[,§]

Structural Biology Group, Department of Physiology, Boston University School of Medicine, 80 East Concord Street, Boston, Massachusetts 02118-2394, and Biology Department, Boston University, Boston, Massachusetts 02215

Received December 2, 1998; Revised Manuscript Received July 16, 1999

ABSTRACT: Class I fructose-1,6-bis(phosphate) aldolase is a glycolytic enzyme that catalyzes the cleavage of fructose 1,6-bis(phosphate) through a covalent Schiff base intermediate. Although the atomic structure of this enzyme is known, assigning catalytic roles to the various enzymic active-site residues has been hampered by the lack of a structure for the enzyme−substrate complex. A mutant aldolase, K146A, is unable to cleave the C3−C4 bond of the hexose while retaining the ability to form the covalent intermediate, although at a greatly diminished rate. The structure of rabbit muscle K146A-aldolase A, in complex with its native substrate, fructose 1,6-bis(phosphate), is determined to 2.3 Å resolution by molecular replacement. The density at the hexose binding site differs between subunits of the tetramer, in that two sites show greater occupancy relative to the other two. The hexose is bound in its linear, open conformation, but not covalently linked to the Schiff base-forming Lys-229. Therefore, this structure most likely represents the bound complex of hexose just after hemiketal hydrolysis and prior to Schiff base formation. The C1-phosphate binding site involves the three backbone nitrogens of Ser-271, Gly-272, and Gly-302, and the ϵ-amino group of Lys-229. This is the same binding site previously found for the analogous phosphate of the product DHAP. The C6-phosphate binding site involves three basic side chains, Arg-303, Arg-42, and Lys-41. The residues closest to Lys-229 were relatively unchanged in position when compared to the unbound wild-type structure. The major differences between the bound and unbound enzyme structures were observed in the positions of Lys-107, Arg-303, and Arg-42, with the greatest difference in the change in conformation of Arg-303. Site-directed mutagenesis was performed on those residues with different conformations in bound versus unbound enzyme. The kinetic constants of these mutant enzymes with the substrates fructose 1,6-bis(phosphate) and fructose 1-phosphate are consistent with their ligand interactions as revealed by the structure reported here, including differing effects on k_{cat} and K_m between the two substrates depending on whether the mutations affect C6-phosphate binding. In the unbound state, Arg-303 forms a salt bridge with Glu-34, and in the liganded structure it interacts closely with the substrate C6-phosphate. The position of the sugar in the binding site would require a large movement prior to achieving the proper position for covalent catalysis with the Schiff base-forming Lys-229. The movement most likely involves a change in the location of the more loosely bound C6-phosphate. This result suggests that the substrate has one position in the Michaelis complex and another in the covalent complex. Such movement could trigger conformational changes in the carboxyl-terminal region, which has been implicated in substrate specificity.

Fructose-1,6-bis(phosphate) aldolases [D-fructose 1,6-bis-(phosphate) D-glyceraldehyde 3-phosphate lyase, EC 4.1.2.13] are ubiquitous glycolytic enzymes that catalyze the reversible aldol cleavage of fructose 1,6-bis(phosphate) (Fru-1,6-P_2)[1] to the triose phosphates glyceraldehyde-3-phosphate (G3P) and dihydroxyacetone phosphate (DHAP). The aldolases catalyze this glycolytic reaction by two distinct mechanisms, which distinguish the enzymes into two classes (*1*). The class I aldolases of animals and higher plants are tetramers of 40 000 dalton subunits with highly conserved amino acid and nucleotide sequences (*2*, *3*). These enzymes utilize covalent catalysis via a Schiff base formed between the enzyme and ketose sugar substrates. The class II aldolases of most bacteria and fungi utilize a divalent metal cation as a cofactor which acts to polarize the ketose carbonyl oxygen, making it a better electron sink for the spread of the developing negative charge during carbon−carbon bond cleavage (*4*). Among the class I enzymes found in vertebrates, three tissue-specific isozymes of aldolases exist: aldolase A (muscle and red blood cells), aldolase B (liver, kidney, and small intestine), and aldolase C (neuronal tissues) (*5*, *6*). The sugar encountered in fructose metabolism,

[†] This work was supported by National Institutes of Health Grant DK43521 (to D.R.T.) and by National Science Foundation Grant MCB-9630430 (to K.N.A.).

[‡] The coordinates of the refined structure have been deposited with the Brookhaven National Laboratories Protein Data Bank, accession code 6ald.

* To whom correspondence should be addressed. E-mail: allen@med-xtal.bu.edu.

[§] Structural Biology Group, Boston University School of Medicine.

[||] Biology Department, Boston University.

[⊥] Current address: Mitotix Inc., 1 Kendall Square, Bldg. 600, Cambridge, MA 02139.

[1] Abbreviations: Fru-1,6-P_2, fructose 1,6-bis(phosphate); G3P, glyceraldehyde-3-phosphate; DHAP, dihydroxyacetone phosphate; Fru-1-P, fructose 1-phosphate; K146A·Fru-1,6-P_2, complex of the mutant aldolase K146A with fructose 1,6-bis(phosphate); Fru-6-P, fructose 6-phosphate; Ins(1,4,5)P_3, inositol-1,4,5-trisphosphate.

10.1021/bi9828371 CCC: $18.00
Published on Web 09/09/1999

fructose 1-phosphate (Fru-1-P), is also a substrate, and the aldolase isozymes display varying degrees of substrate specificity between Fru-1,6-P_2 and Fru-1-P. This differential activity has been used as a basis for discriminating among these vertebrate isozymes in tissues and in the diagnosis of a variety of disease states, e.g., liver damage, cancer, and hereditary fructose intolerance (*7*−*9*). An understanding of the enzyme mechanism by which the aldolase isozymes catalyze their reactions will require structures with inhibitors bound as well as substrates productively bound in the active site. Such an understanding is key to the design of inhibitors, such as one for the malarial aldolase, whereby preferential inhibition would lead to an effective treatment for the disease (*10*, *11*). Detailed mechanistic insight will also be crucial for explaining the pathology of genetic disorders caused by mutations in aldolases: aldolase-deficient hemolytic anemia and hereditary fructose intolerance (*9*).

The catalytic mechanism has been most extensively studied using the class I aldolase A from rabbit muscle (*4*). On the basis of a great deal of experimental evidence, it is clear that the aldol cleavage proceeds through a number of distinct enzyme−substrate intermediates, including a carbinolamine, imine (Schiff base), and an enamine/carbanion (*4*, *12*, *13*). With the exception of the Schiff base-forming Lys-229 (*14*), the role of essential amino acid residues in the active site is equivocal or completely unknown (*15*−*17*). The unliganded structures of Fru-1,6-P_2 aldolases from rabbit (*16*) and human muscle (*18*) and nonvertebrate aldolases from *Drosophila melanogaster* (*19*) and *Plasmodium falciparum* (*11*) have been determined. The molecular architecture of the enzyme has revealed possible residues involved in the catalytic cycle (*16*); however, there is a dearth of three-dimensional structures of liganded enzyme. A recent report of a complex with DHAP, one of the product trioses, has localized this three-carbon sugar in three alternate conformations (*20*). Using site-directed mutagenesis, many of the residues around Lys-229 have been investigated, and differing effects on the rates of formation and/or equilibria of the enzyme−substrate intermediates have been observed and used as a basis for interpreting the roles of various residues. However, these results can be misleading and difficult to interpret (*17*, *21*−*23*).

The lack of tightly bound inhibitors (*24*) and the activity of the enzyme in the crystalline state (*25*) have made crystallization of liganded complexes difficult. To elucidate the roles of various residues in and around the active site, we have chosen the dual approach of X-ray crystallography in conjunction with site-directed mutagenesis of rabbit aldolase A. In this report we use the K146A mutant form of rabbit aldolase A in the crystalline state bound to the natural substrate Fru-1,6-P_2. This mutant enzyme cannot turn over the substrate due to the inability to catalyze cleavage of the carbon−carbon bond. However, K146A retains the ability to make the Schiff base intermediate (*17*). The structure reveals the bound hexose in the open chain form as it would exist in the active site prior to formation of the first covalent intermediate. Characterization of several site-directed mutants supports the interpretation of the structure and the role of several residues in the binding of Fru-1,6-P_2. These results, in conjunction with the recently reported structure of human muscle aldolase A bound to Fru-1,6-P_2 (*26*) in an alternative binding mode, suggest a rearrangement of the substrate prior to Schiff base formation.

MATERIALS AND METHODS

Materials. Glycerol-3-phosphate dehydrogenase/triose phosphate isomerase were purchased from Boehringer/Mannheim. Cm-Sepharose CL-6B Fast Flow, Superose-12, and Sephadex G-150 were from Pharmacia. Oligonucleotides for site-directed mutagenesis and sequence determination were synthesized on Milligen/Biosearch DNA synthesizers using phosphoramidite chemistry and the manufacturers' protocols. When necessary, oligonucleotides were purified by urea−PAGE. Fru-1,6-P_2, Fru-1-P, and other chemicals were from Sigma Chemical Co. or Fluka.

Site-Directed Mutagenesis, Expression, and Purification of Mutant Aldolases. E. coli strains JM103 and TG1 were used for M13 cloning and mutagenesis. JM83 and DH5α were used for expression. Site-directed mutagenesis was performed to change Glu-34 (GAG) and Arg-303 (CGT) codons to Ala using the oligodeoxyribonucleotides: 5′-CTGCAGATGCGTCGACCGG (E34A) and 5′-CTCCTACGGCGCTGCCCTGCAG (R303A). The potential mutants were screened by DNA sequence determination using dideoxy-termination (*27*). Sequence determination employed 7-deaza-dGuo triphosphate in place of dGTP, which alleviated much of the G/C compression present in the rabbit aldolase A sequence (*28*). Expression of both wild-type and mutant aldolases was done in bacteria as described previously (*21*). Purification of both wild-type and mutant enzymes was the same, except that R303A-aldolase was eluted from the Cm-Sepharose at a lower pH (7.8 instead of 8.3) and used MOPS in place of TAPS. Aldolase containing fractions from the affinity elution of Cm-Sepharose or from subsequent filtration on Sephadex or Superose were pooled and precipitated in 65% saturated ammonium sulfate. Protein suspensions were stored at 4 °C.

Enzyme Analysis. SDS−PAGE (12.5%) was performed, and gels were stained with Coomassie R-250 [0.1% in water/methanol/acetic acid (5:5:1)] (*29*). Protein concentration was determined by dye binding using bovine serum albumin as a standard, or for pure aldolase by absorbance using E_{280}-(0.1%) = 0.91 (*30*). The substrate cleavage rate was determined by measuring the decrease in absorbance per minute at 340 nm in a coupled assay (*31*). Aldolase was diluted in 50 mM TEA·HCl, pH 7.4, and added to a cuvette containing 50 mM TEA·HCl, pH 7.4, 10 mM EDTA, 0.16 mM NADH, 10 μg/mL glycerol-3-phosphate dehydrogenase/triose phosphate isomerase (10:1). Assays of 1.0 mL were performed in triplicate at 30 °C following addition of substrate. The cleavage rate for Fru-1,6-P_2 was measured over a substrate concentration range of 1.25−300 μM, with 0.3 μg of wild-type enzyme, or up to 100 μg of the mutant enzymes. The cleavage rate for Fru-1-P was measured over a substrate concentration range of 5−50 mM, with 23 μg of wild-type enzyme, or up to 600 μg of the mutant enzymes. Kinetic values were determined from double reciprocal plots using a least-squares method that explicitly included the errors in rate measurement as weights (*32*).

Crystallization. Although crystallization conditions for rabbit muscle aldolase have been reported (*16*), new crystallization conditions were developed in order to avoid the use of ammonium sulfate as precipitant (since sulfate sometimes binds in the active site of enzymes when present in high concentrations). The crystallization conditions known for

aldolase from *Drosophila melanogaster* (*19*) were used as starting conditions for optimization. Crystals were grown using hanging drop geometry and the vapor diffusion method. The protein solution consisted of 7 mg/mL aldolase dissolved in 0.1 M Tris·HCl, pH 7.4, 1 mM EDTA, 1 mM β-mercaptoethanol, 1 mM DTT. A drop (5 μL) of the protein solution was mixed with an equal volume of drop buffer consisting of 0.1 M Tris·HCl, pH 7.4, 0.1 mM DTT, 1 mM β-mercaptoethanol, 1 mM EDTA, and 10% PEG 6000 at 4 °C and suspended over a well containing 1.0 mL of a solution containing 0.1 M Tris·HCl, pH 7.4, 24% PEG 6000 at 4 °C. Crystals grew at 4 °C in 1−2 weeks in the form of plates with dimensions of 0.5 × 0.4 × 0.05 mm. The space group is $P2_1$ with unit cell dimensions $a = 82.8$ Å, $b = 100.6$ Å, $c = 84.5$ Å, and $\beta = 98.3°$. Crystals of suitable quality were soaked overnight in substrate by slowly exchanging (2 μL additions and removals over 1 h) the mother liquor for a soak solution consisting of the drop buffer described above plus 5 mM Fru-1,6-P_2, trisodium salt octahydrate (Fluka) and 15% 2-methyl-2,4-pentanediol. The soak solution also serves as a cryoprotectant.

Data Collection. Data were collected by freezing the cryoprotected soaked crystal directly in a stream of nitrogen cooled to −180 °C using CuKα radiation from a Rigaku RU300 rotating anode X-ray generator equipped with a Raxis-II imaging plate area detector. A crystal-to-detector distance of 120 mm and 1° oscillations were used. The autoindexing routine in DENZO was used to determine the unit cell constants (*33*). The programs DENZO and SCALEPACK were used to index and reduce the data, respectively. The assignment to $P2_1$ was made by assessing systematic absences. The data set, obtained from a single crystal, was 95% complete to 2.3 Å resolution with an I/σ ratio of 2.4 in the highest resolution shell.

Structure Determination. The initial phase information was determined by molecular replacement using the program AMoRe from the CCP4 program suite (*34, 35*). The number of molecules in the asymmetric unit was calculated to be 4 [assuming a Matthews constant of 2.3 Å^3 Da^{-1} (*36*)]. The self-rotation function calculated with the program GLRF (*37*) using data in the resolution range 10−4 Å gave results consistent with the *222* symmetry revealed in previous crystal structures of Fru-1,6-P_2 aldolase (*16, 19*). The probe structure used was the backbone of the aldolase tetramer (pdb accession code 1ado) comprised of residues 1−343 from the 1.9 Å structure by Blom and Sygusch (*20*). A sphere radius of 40 Å and data from 20.0 to 4.0 Å resolution with $F/\sigma(F) > 0$ were used in rotation and translation function calculations. The molecular replacement solution provided an initial structural model with a crystallographic $R = 42.3$. The tetramer model including side chains was then rotated and translated using the molecular rotation solution and subjected to refinement.

Refinement. Five percent of all reflections were excluded from the refinement for the calculation of the free *R*-factor (*38*). Rigid-body refinement was performed in the program X-PLOR (*39*) defining each monomer as a rigid body to refine the noncrystallographic symmetry (NCS) operators. The NCS operators were then calculated from the model output by X-PLOR using the lsq_explicit routine in the graphics program O (*40*). These symmetry operators were used to impose strict NCS constraints in the first two rounds of refinement and model building using the program X-PLOR. Each round of refinement included rigid-body, positional, preparational, and slow-cooling ($t = 3000$ K) refinement protocols followed by manual rebuilding on a Silicon Graphics O2 Workstation using the graphics program O. NCS-averaged electron density maps were calculated using the RAVE program package (*41*). The protein model was built into density in the NCS-averaged $2F_o - F_c$ maps contoured at 1.2 σ. Building was also guided by $F_o - F_c$ maps with electron density contoured at 1.0 and −1.0 σ.

Subsequent rounds of refinement (after the crystallographic *R*-factor and *R*-free had dropped below 0.3) were performed using NCS restraints with a high weight (300 kcal mol^{-1} Å^{-2}). Water molecules (385 in total) were added to the model using a $F_o - F_c$ map with electron density contoured at 3 σ. In the final round of refinement, the model of Fru-1,6-P_2 was added using a $2F_o - F_c$ map averaged over two of the four monomers (see Results and Discussion section). Topology and parameter files for Fru-1,6-P_2 were generated using the xplor2d program in the CCP4 suite (*35*) and modified using parameters obtained from the energy-minimized structure of Fru-1,6-P_2 in the program QUANTA97 (MSI, Inc.). The final structure had an *R*-factor of 0.228 and a free *R*-factor of 0.274 using data in the resolution range 100.0−2.3 Å and no F/σ intensity cutoff. The final structure contains residues 2−344, 385 water molecules, and 2 Fru-1,6-P_2 molecules. The model included residue 344 as a Pro (*42, 43*), which Blom and Sygusch (*20*) had assigned as a Ser based on electron density (accession code 1ado). The geometric parameters of the model have been analyzed with PROCHECK (*44*) and are within the expected deviations from ideality calculated from other structures determined to 2.3 Å resolution. The coordinates have been deposited with the Protein Data Bank (accession code 6ald) and are also available from the corresponding author upon request.

RESULTS AND DISCUSSION

Structure Determination. The rabbit muscle K146A-aldolase A, in complex with Fru-1,6-P_2, crystallizes in the space group $P2_1$ with four monomers per asymmetric unit. The crystal structure was determined by molecular replacement (Table 1) and refined to 2.3 Å resolution with a crystallographic *R*-factor of 0.228 and a free *R*-factor of 0.274. The Ramachandran plot shows that 89% of the residues are in the "favored" regions defined by PROCHECK, with the remaining 11% of the residues falling in the "allowed" regions. The structure is well-defined with an average *B*-factor of 26.2 Å^2 for both main-chain and side-chain atoms. The final model comprises protein residues 2−344, a total of 385 water molecules in the tetramer, and 2 Fru-1,6-P_2 molecules in 2 of the 4 monomers. The 19 C-terminal residues are too disordered to be accurately modeled. For other structures of aldolase, the C-terminal region (residues 345−363) was disordered with no model for this region included (*11, 16*). Two previously published structures that include the 19 C-terminal residues, *Drosophila* aldolase (*19*), and DHAP-bound rabbit aldolase A (*20*) (pdb entries 1ald and 1ado, respectively) place the C-terminal region in different conformations. The C-terminal region of Fru-1,6-P_2 aldolase has been implicated in substrate binding in biochemical studies involving chemical modification (*45*), truncation (*46−48*), and site-directed mutagenesis (*49, 50*).

Table 1: Data Collection and Refinement Statistics

Data Collection	
resolution	∞−2.3 Å
reflections	62360
completeness (outer shell) (%)	95.3
R_{sym} (inner shell/outer shell)[a]	0.097/0.182
I/σ (outer shell)	2.4
Refinement Statistics	
protein atoms (non-hydrogen)	10456
no. of water molecules	385
no. of Fru-1,6-P_2 molecules	2
resolution	100.0−2.3
σ cutoff	0
crystallographic *R*-factor	0.228
free *R*-factor[b]	0.274
mean *B*-factors (Å^2)	26.21
rms deviation	
bonds	0.004
angles	1.117
dihedrals	25.238
impropers	0.619

[a] $R = \sum[(I - <I>)^2]/\sum I^2$. [b] The free *R*-factor (*38*) was calculated from a random selection constituting 5% of the data.

More recently, many of the isozyme-specific residues in vertebrate aldolases have been located in the C-terminal region (*51, 52*). The inability to satisfactorily localize the C-terminus has largely been attributed to conformational changes in the protein upon substrate binding and the limitations of crystallographic experiments in which the substrate is soaked into existing crystals (i.e., protein motion is restricted by crystal contacts or soaking conditions).

Protein Structure. As is consistent with the tight noncrystallographic symmetry restraints used during refinement, the monomers comprising the tetramer are nearly identical to one another with a root-mean-squared (rms) deviation of 0.008 Å. Both the tertiary fold of the monomer and the relative orientation of the monomers in the tetramer in the aldolase−substrate complex are similar to those of the native human aldolase (*18*), which indicates that no gross conformational changes occur upon mutation of K146A and/or binding of substrate. The rms deviation for the common 343 Cα atoms (excluding the disordered C-terminus) between the native human enzyme and this complex is 0.331 Å. The protein structure is also similar to the rabbit muscle aldolase complexed with DHAP (*20*) with an rms deviation for the 343 common Cα atoms of 0.337 Å. Structural changes due to the mutation of K146A and/or substrate binding for the observed residues are therefore restricted to side-chain movements.

Substrate Binding and Orientation. The electron density in the Fru-1,6-P_2 binding site is different among subunits (called here monomers A, B, C, and D) of the tetramer, with two subunits showing clearer electron density for the substrate relative to the other two. To test whether the ligand was bound to these subunits in the same relative orientation, electron density maps were averaged over all possible pairs of monomers and the tetramer as described under Materials and Methods. The electron density map made by averaging over monomers A and B showed clear electron density for the substrate (see Figure 1) while the maps made by averaging over monomers C and D showed little density in the active site. The K146A·Fru-1,6-P_2 complex was therefore built with a model for Fru-1,6-P_2 in the active sites of only monomers A and B. One interpretation of this result is that there is half-site reactivity in Fru-1,6-P_2 aldolase. The observation of such half-site reactivity is precedented by biochemical studies of Fru-1,6-P_2 aldolase at low temperatures with DHAP as substrate (*53*−*55*). This is consistent with the observed X-ray crystallographic structures of this K146A·Fru-1,6-P_2 complex and the aldolase−DHAP complex (*20*). In both structures, the Fru-1,6-P_2 and DHAP, respectively, were found in the same two monomers of the tetramer. The oligomeric organization and/or monomeric structure of Fru-1,6-P_2 aldolase does not provide structural evidence to explain why one dimer pair (A−B) binds substrate in a structurally ordered fashion and the other pair does not.

The Fru-1,6-P_2 is bound, but not covalently linked, to the Schiff base-forming Lys-229. This finding is consistent with the kinetic studies of K146A-aldolase against the substrate Fru-1,6-P_2. K146A is capable of forming the Schiff base with Fru-1,6-P_2, albeit at a greatly reduced rate compared to the native enzyme (10^4-fold slower). The K146A mutant does not catalyze the C−C bond cleavage reaction (*17*). Thus, the substrate species bound to K146A when Fru-1,6-P_2 is soaked into crystals of the mutant enzyme is expected to be either the unreacted Schiff base or the Michaelis enzyme−substrate complex formed before the covalent Schiff base adduct is made. The observed density is thus consistent with the latter possibility. Alternatively, if Lys-146 were essential for catalysis of ring-opening, then the cyclic form of the sugar (β anomer) might be observed. Models for cyclic α- and β-Fru-1,6-P_2 pyranose from the protein data bank (accession code 1fbh) were fit into the observed electron density in the active site of the K146A·Fru-1,6-P_2 complex. Neither the α nor the β anomer fit the electron density as well as the linear form of the sugar. The Fru-1,6-P_2 is bound in its linear, extended form with the C1-phosphate group in the vicinity of Lys-229 and the C6-phosphate near Arg-303. Although the ligand density alone cannot be used to distinguish the C1-phosphate from the C6-phosphate, the model was built with the orientation that allowed the closest proximity of the C2-carbonyl to Lys-229 and which was consistent with the position of the analogous phosphate in the DHAP-bound structure (*20*). Figure 2 is a schematic representation of Fru-1,6-P_2 binding including interatomic distances between hydrogen bond donors and acceptors of substrate and protein. The C1-phosphate binding site is made of backbone nitrogens of Ser-271, Gly-272, and Gly-302 and the ϵ-amino of Lys-229. The groups proximal to the phosphate oxygens are potential proton donors, which is consistent with a fully ionized phosphate. The residues Asp-33 and Glu-187 also make hydrogen bonds to the C1-phosphate group via water molecules. The phosphoester oxygen O1 makes a hydrogen bond to the backbone nitrogens of Gly-302 and Gly-272 and the hydroxyl of Ser-271. In comparison, the number of interactions made to the C6-phosphate of Fru-1,6-P_2 are fewer and involve three conserved basic side chains: Lys-41, Arg-42, and Arg-303. This structural evidence, which shows interactions with flexible protein side chains rather than the main chain, suggests that the C6-phosphate may not bind as tightly as the C1-phosphate. This result is also consistent with substrate specificity studies which show that Fru-1,6-P_2 aldolase catalyzes the bond cleavage of Fru-1,6-P_2 and Fru-1-P, but not fructose 6-phosphate (Fru-6-P) (*24*).

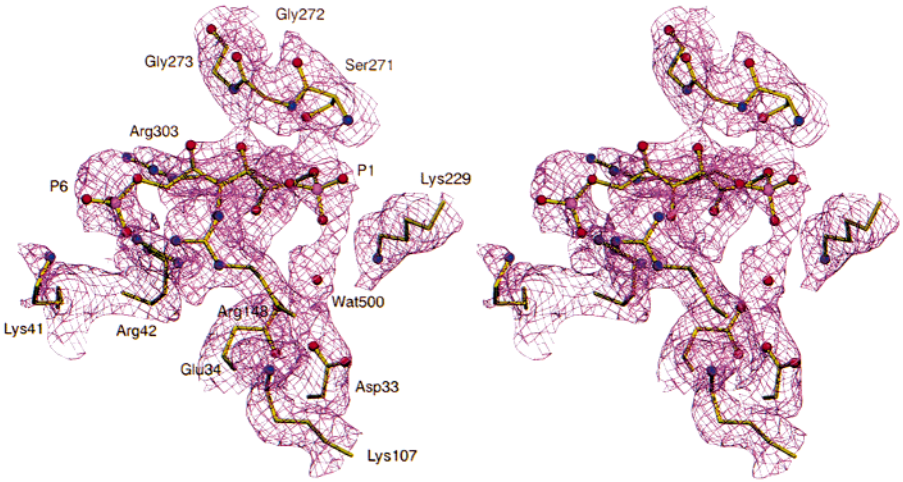

FIGURE 1: Stereoview of electron density showing Fru-1,6-P_2, surrounding residues, and ordered water. The C1- and C6-phosphate groups are labeled P1 and P6, respectively. The electron density from a $2F_o - F_c$ omit map (contoured at 1.0 σ) averaged over monomers A and B is depicted as magenta cages while the atomic coordinates are depicted as ball-and-stick models. This figure was rendered using the programs MOLSCRIPT (*70*) and POV-Ray (Persistence of Vision Ray Tracer, Version 3.01).

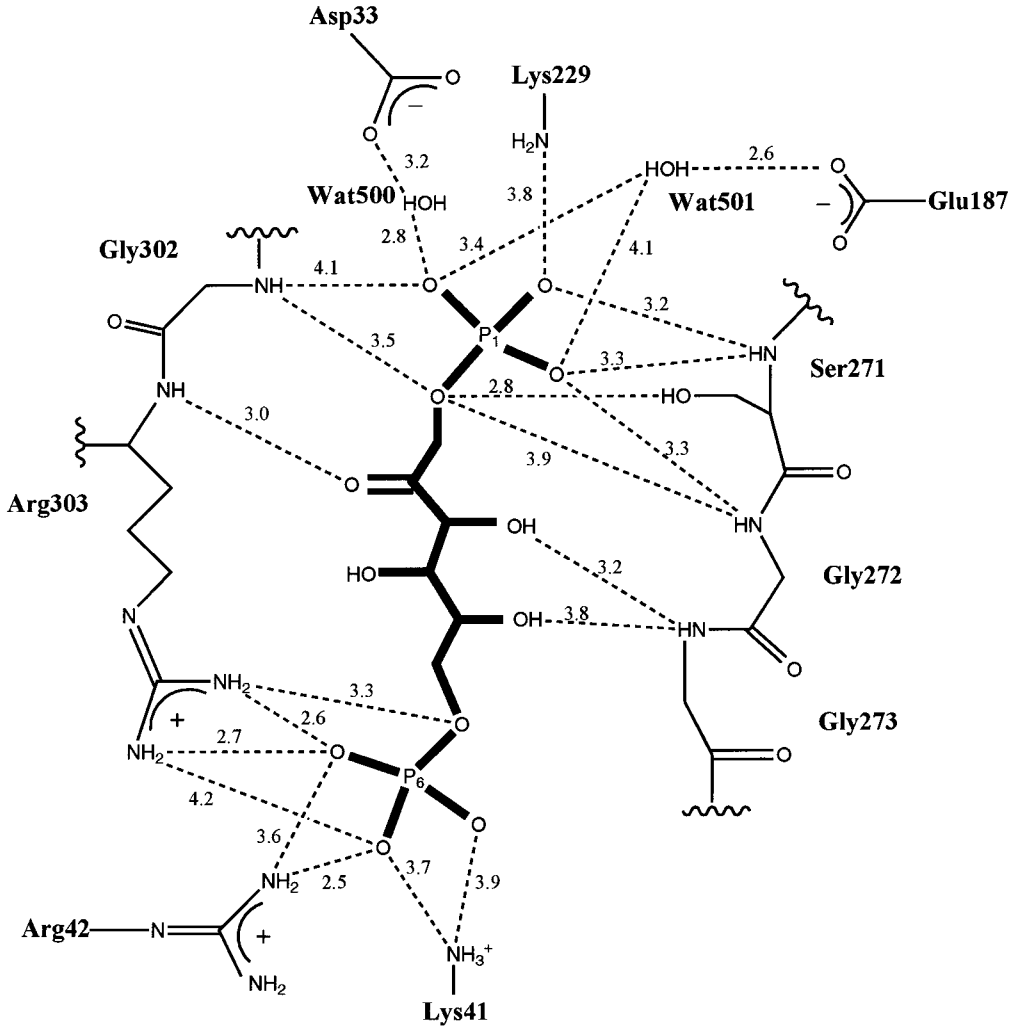

FIGURE 2: Schematic representation of the enzymic amino acids interacting with the substrate Fru-1,6-P_2 in the K146A active site. Potential hydrogen bonds between the substrate and groups within 4.0 ± 0.3 Å are denoted by dashed lines.

Perhaps the lack of catalytic activity against Fru-6-P, which is an inhibitor but not a substrate for the enzyme, is the result of poor alignment of the substrate in the active site, with the C6-phosphate binding at the C1-phosphate binding site (nonproductive binding).

Substrate binding does not depend solely on the binding of the substrate phosphate groups to enzyme. Fru-1,6-P_2 also binds the enzyme via interactions with the sugar carbonyl and hydroxyl groups. The substrate C2-carbonyl makes a hydrogen bond to the backbone nitrogen of Arg-303 while

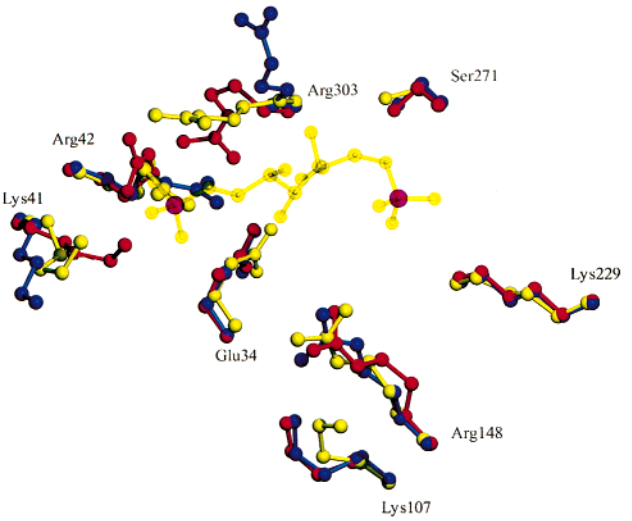

FIGURE 3: Superposition of the active sites of the K146A·Fru-1,6-P_2 complex (yellow), unbound human aldolase (red), and aldolase−DHAP complex (blue) depicted with ball-and-stick models. The Fru-1,6-P_2 is shown in yellow. The catalytic Lys-229 is shown for reference. With respect to its position in the K146A structure, Arg-303 of the unbound structure is rotated out of the binding site and makes a hydrogen bond to Glu-34. This figure was rendered using the programs MOLSCRIPT (*70*) and POV-Ray (Persistence of Vision Ray Tracer, Version 3.01).

the C3- and C5-hydroxyl groups of Fru-1,6-P_2 each make a hydrogen bond to the backbone nitrogen of Gly-273, which may account for some of the stereospecificity at C3 (*56*−*58*).

The average *B*-factor for the substrate is 65.4 Å^2, which is not unexpected since the *B*-factors of side chains in the vicinity of the binding site are similar to this (40−70 Å^2) in the DHAP-bound aldolase. The *B*-factors probably reflect an occupancy of less than 1.0, which was the value for occupancy used in the refinement. A lower than 100% occupancy could be attributed to the fact that the substrate concentration may have been lower than required since the K_m for K146A is unknown (*17*), although the concentration used was 250 times the wild-type K_m.

Site-Directed Mutagenesis of Residues Involved in Substrate Binding. The possibility that this structure represents a nonproductive binding mode was addressed by site-directed mutagenesis of residues unique to this site. These include the side chains of Arg-303 and Arg-42, which are part of the C6-phosphate binding site. The kinetic results were compared to those for site-directed mutants of alternative C6-phosphate binding residues previously proposed (*59*, *60*). Arg-303 is the residue that shows the greatest change in conformation upon binding (see section below and Figure 3). In the unbound structure, Arg-303 forms a salt bridge with Glu-34 (*16*), and in the liganded structure, it interacts closely with the substrate C6-phosphate. Single-site mutants of Arg-303 and Glu-34 were made. Using purified mutant protein, the kinetic constants were determined and compared to wild type and other previously published mutations (*61*) involving this and other previously proposed C6-phosphate sites (Table 2). The Arg-303 to Ala mutation has a considerable effect on k_{cat}/K_m (400-fold decrease) and is comparable to similar mutations made (*61*) at other residues previously proposed to be implicated in binding from chemical modification studies, such as Lys-107 (*60*) and Arg-148 (*59*). The importance of Arg-303 in catalysis is consistent with the structure of the mutant enzyme with Fru-1,6-P_2 bound, which shows Arg-303 binding two C6-phosphate oxygens and the C6-phosphoester oxygen. The Glu-34 mutation has only a slight effect (14-fold) on k_{cat}/K_m, which is consistent with the more indirect role it plays by making a salt bridge in the unbound enzyme. R42A has a comparable decrease in k_{cat}/K_m to E34A, indicating that this residue may not interact as strongly with the substrate or that Arg-303 has a dominant role in binding. In the K146A·Fru-1,6-P_2 complex structure, there are two possible hydrogen bonds from Arg-42 to the C6-phosphate (Figure 3).

The role of these residues in the C6-phosphate binding site was tested further by analysis of the kinetics of the mutant enzymes toward Fru-1-P as substrate, which obviously lacks the C6-phosphate group (Table 3). The result for R303A is that, while the fold change in k_{cat}/K_m with Fru-1-P is nearly the same as for Fru-1,6-P_2, the effect is due to the difference in k_{cat}, not in K_m. The K107A, R148A, and E34A mutants had the same K_m as wild-type enzyme with Fru-1-P, and the K_m for R303A and R42A with Fru-1-P was only slightly higher than that for wild type. While K_m is not necessarily equivalent to the binding constant, the changes are consistent with both the structure here and the structure of aldolase A bound to Fru-1,6-P_2 recently published (*26*), indicating that these residues are all involved in C6-phosphate binding. The lack of a significant change in K_m for Fru-1-P in these mutant enzymes also indicates that it is unlikely that there is a unexplained structural rearrangement of the protein due to these mutations. The fold decreases in k_{cat} for the R303A, E34A, and R42A mutant enzymes are similar for Fru-1,6-P_2 and Fru-1-P, while the fold decreases in k_{cat} for K107A and R148A are less for Fru-1-P compared to Fru-1,6-P_2. It is noteworthy that the K107A mutant enzyme appears to behave identically to wild type in both K_m and k_{cat} with Fru-1-P as substrate. The K_m results indicate that both Lys-107 and Arg-148 play a role in interactions with C6-phosphate sometime during the catalytic cycle, which is consistent with the ligand binding site in a structure recently determined (*26*). The k_{cat} results indicate that, with the exception of Lys-107 and Arg-42, all the mutated residues are involved in rate-limiting steps in the catalytic cycle common to both substrates, such as product release (*12*, *17*, *22*).

Both the liganded structure and the site-directed mutagenesis results indicate that Arg-303 plays an important role in the aldolase mechanism. In addition, previous modeling studies using the unliganded human aldolase A have implicated Arg-303 in substrate binding (*62*). Arg-303 has been proposed to be involved in binding the cyclic form of the substrate (*26*). Furthermore, it is interesting that a naturally occurring mutation in aldolase B that causes hereditary fructose intolerance has been identified as Arg-303 substituted with Trp (*9*). Although the possibility exists that the crystal contacts or the K146A mutation are responsible for stabilizing the binding mode observed here, this structure is consistent with the kinetic data and can be explained in the context of other structures.

Comparison with Unbound Enzyme and Enzyme−Product Complex. As described in the section on protein structure, there are no gross conformational changes in the K146A·Fru-1,6-P_2 complex caused either by the mutation or by

Table 2: Steady-State Rates of Fru-1,6-P_2 Cleavage for C6-Phosphate Binding Site Mutants

aldolase	k_{cat} (s^{-1})	fold decrease	K_m (μM)	fold increase	k_{cat}/K_m (M^{-1} s^{-1})	fold change
wild type[a]	14 ± 0.3	–	14.3 ± 0.7	–	980000± 50000	–
R303A	0.61 ± 0.05	23	250 ± 21	17	2400 ± 200	400
R42A[b]	6.8 ± 0.3	2	45 ± 5	3	151000 ± 17000	7
E34A	2.2 ± 0.1	6	32 ± 3	2	69000 ± 6500	14
K107A[b]	0.235 ± 0.007	60	170 ± 12	12	1400 ± 100	700
R148A[b]	0.2077 ± 0.00005	70	141 ± 7	10	1470 ± 70	670

[a] (*21*). [b] (*61*).

Table 3: Steady-State Rates of Fru-1-P Cleavage for C6-Phosphate Binding Site Mutants

aldolase	k_{cat} (s^{-1})	fold decrease	K_m (mM)	fold increase	k_{cat}/K_m (M^{-1} s^{-1})	fold change
wild-type[a]	0.37 ± 0.07	–	6.5 ± 2	–	60 ± 20	–
R303A	0.0062 ± 0.0007	60	19 ± 2	3	0.33 ± 0.05	100−300
R42A	0.17 ± 0.04	2	14 ± 4	2	12 ± 4	3−10
E34A	0.055 ± 0.009	7	9.9 ± 0.7	1	5.6 ± 1.0	10
K107A	0.36 ± 0.03	1	6 ± 1	1	60 ± 10	–
R148A	0.023 ± 0.002	15	9.5 ± 1.0	1	2.4 ± 0.3	25

[a] Values indicated here are similar to those published elsewhere (*6*, *21*).

binding of the natural substrate Fru-1,6-P_2. The Fru-1,6-P_2 binding site itself overlaps the binding site found for the product DHAP molecules visualized in the previously published DHAP structure (*20*). In the published structure, two of the three alternate orientations of DHAP are located in the same enzyme monomer, and the third DHAP is similar in location to one of the other two. Thus, in that structure there are two major conformations for DHAP; however, all three DHAP models possess a common location for the binding of the C1-phosphate group, which coincides with the binding site for the C1-phosphate of Fru-1,6-P_2 in the K146A·Fru-1,6-P_2 complex. The monomer with the two alternate DHAP binding modes was chosen for comparison to the K146A·Fru-1,6-P_2 complex. Figure 3 shows the K146A·Fru-1,6-P_2 complex superimposed with the aldolase−DHAP complex, excluding the DHAP ligand. Also superimposed is the unbound human aldolase structure (*18*). The positions of Ser-271 and Lys-229 residues which bind the C1-phosphate in all the liganded models do not differ significantly in all three structures. Thus, no movement of these residues is necessary to accommodate either the Michaelis complex with Fru-1,6-P_2 or the enzyme−product complex relative to the native enzyme conformation. The fact that Lys-229 does not shift position is important to the argument that the K146A mutation has not caused a movement of this essential catalytic nucleophile from that conformation normally adopted (although it is possible that the Michaelis complex may have adopted a different conformation were there no mutation). A much more profound rearrangement of the residues comprising the C6-phosphate binding site was observed.

In the C6-phosphate binding site observed in the K146A·Fru-1,6-P_2 complex, there are movements in the side-chain conformations of residues involved in binding relative to their positions in unbound enzyme and enzyme−product complex (Figure 3). The side chains of Lys-41, Arg-42, and Arg-303 are changed in position such that their terminal amino or guanidino groups are pointed toward the C6-phosphate of Fru-1,6-P_2. The largest such movement occurs in the side chain of Arg-303, which in the native structure is folded back from the active site forming a salt bridge with Glu-34. In the K146A structure, Lys-41 is pulled toward the C6-phosphate of substrate and is closer to Arg-42, while in the DHAP structure Lys-41 is pointed away from the substrate/product binding site. The difference in position is not as great for Arg-42. Notably, this residue makes a hydrogen bond to Glu-34 in the DHAP-bound structure (as opposed to the Arg-303/Glu-34 pair in the unbound structure). In contrast, Arg-148, which is not close enough to interact electrostatically with the bound Fru-1,6-P_2, does not change position significantly in the K146A·Fru-1,6-P_2 complex when compared to the unbound and product-bound structures and makes an ion-pair with Glu-189 (not shown).

The rate-limiting or partially rate-limiting step in Fru-1,6-P_2 cleavage has been proposed to be product release (*12*, *17*, *22*), but a partially rate-limiting conformational change has also been suggested (*25*, *63*). The conformational change hypothesis is especially attractive since residues in the C-terminus of aldolase have been shown to be important to catalytic activity (*45*, *47*, *49*), and since the C-terminus appears to be extremely mobile [since it is either absent or appears in different positions in X-ray crystallographic structures (*16*, *19*, *20*)]. In the DHAP-bound structure, Arg-303 makes a salt bridge with a residue in the C-terminus, Glu-354, replacing the Arg-303/Glu-34 pair observed in the unliganded structure. The rearrangement of Lys-41, Arg-303, and Glu-34 upon binding of Fru-1,6-P_2 (and subsequent rearrangement upon C−C bond cleavage and dissociation of the first product G3P) could be the trigger for the change in conformation of the C-terminus, which might explain the k_{cat} effects seen with the R303A mutant enzyme, and to a lesser extent E34A, toward both Fru-1,6-P_2 and Fru-1-P (Tables 2 and 3). Figure 4 shows the electrostatic potential surface for the native and K146A·Fru-1,6-P_2 structures with Fru-1,6-P_2 depicted in the mutant structure (Fru-1,6-P_2 molecule excluded from electrostatic surface calculation). A positively charged active-site cleft is clearly visible in both structures. In the native structure, the Arg-303 residue is part of a surface with a net neutral electrostatic charge (partly due to the interaction of Arg-303 with Glu-34). In the

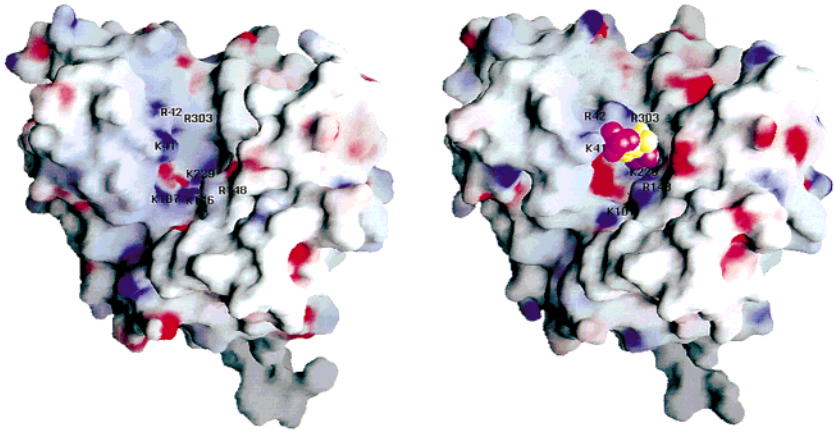

FIGURE 4: Electrostatic potential surface of native human aldolase (left) and the K146A·Fru-1,6-P_2 complex (Fru-1,6-P_2 not included in the calculation) with Fru-1,6-P_2 shown as a yellow space-filling model with purple phosphate groups (right). The protein electrostatic surface was contoured at −15 kT (red, most negative) and +35 kT (blue, most positive). The active site and phosphate binding site residues are labeled. Upon binding of Fru-1,6-P_2, the active site is partially occluded by movement of Arg-303. All surfaces were calculated and displayed using the program GRASP (*71*).

liganded structure, the Fru-1,6-P_2 sugar molecule is partially occluded by the side chain of Arg-303 which has moved to close over the active site and the substrate. Because the salt bridge with Glu-34 is broken, Arg-303 shows a net positive charge. The rearrangement of the side chains involved in the binding of the C6-phosphate of Fru-1,6-P_2 has not perturbed significantly the calculated electrostatic surface potential with respect to the native or DHAP-bound complex (not shown). The mutation of Lys-146 to Ala did not significantly change the calculated electrostatic surface potential of aldolase, except for an extremely localized effect making the pocket less positively charged.

Implications for the Catalytic Mechanism. While this manuscript was in preparation, the crystal structure of wild-type human muscle aldolase A complexed with Fru-1,6-P_2 was reported to 2.8 Å resolution (*26*). The rabbit and human muscle enzymes are identical for all intents and purposes: there are 5 amino acid substitutions in the 363 residue primary sequence, an extremely low (0.331 Å) rms deviation in the crystal structures, and no significant difference in the kinetic constants. Like the structure reported here, the human muscle aldolase A·Fru-1,6-P_2 complex was obtained by soaking preformed crystals in a solution of Fru-1,6-P_2. Furthermore, the complex observed for the human aldolase A also reveals the linear form of the sugar bound noncovalently in the active site. Although the enzymes in the K146A and in the human aldolase A complexes are capable of catalyzing Schiff base formation, a significant amount of Schiff base does not accumulate during the soak time of these X-ray diffraction experiments (8 h for K146A·Fru-1,6-P_2 and several days for the human enzyme). In the mutant K146A, the rate of Schiff base formation is 27 000-fold decreased compared to wild type (*17*). The rate of conversion to the Schiff base may be significantly slower in the crystal, especially if Schiff base formation is preceded by some alterations in the enzyme conformation. Such an argument would explain the lack of Schiff base formation in both Fru-1,6-P_2 complexes. It should be noted, however, that the two aldolase−hexose complexes were grown under different crystallization conditions and yielded different space groups.

The binding mode for substrate found in the human aldolase A·Fru-1,6-P_2 complex (*26*) shows the same C1-phosphate binding site found in the K146A·Fru-1,6-P_2 complex (backbone nitrogens of Ser-271 and Gly-272). However, the C6-phosphate binding subsite is distinct and includes the side chain of Lys-107 in the human aldolase structure. Thus, the two Fru-1,6-P_2-bound aldolase structures are inconsistent with regard to the C6-phosphate binding sites. Arguments could be made that either one or both represent unproductive complexes that are not mechanistically relevant. The mutagenesis of Lys-107 and the different kinetic effects toward the two hexose substrates (Tables 2 and 3) support that the conformation of hexose with the C6-phosphate near Lys-107 is productive. Likewise, the evolutionary conservation of Arg-303 (*52*), its implication as a phosphate binding site for Ins(1,4,5)P_3 (*64*), its identification in an inactivating R303W mutation in aldolase B that causes disease (*9*), and the loss of activity upon mutation (Tables 2 and 3) are all evidence for the involvement of Arg-303 in the mechanism. From these lines of evidence it is most likely that the K146A·Fru-1,6-P_2 structure represents a kinetically relevant conformation of the substrate. If both complexes are therefore relevant to the mechanism, two binding modes for hexose must occur during the catalytic cycle.

As mentioned above, the binding site revealed by the structure of this K146A·Fru-1,6-P_2 complex does not position the substrate in the proper orientation for catalysis via a Lys-229−substrate adduct. There is biochemical evidence that ring opening occurs after binding to the enzyme (*65*, *66*), although this anomerase activity of aldolase A is equivocal (*67*, *68*). The fact that binding at the subsite presented here is distinct from that required for cleavage might indicate that it could be the site for ring opening. The K146A·Fru-1,6-P_2 structure indicates that the movement of the substrate into the catalytic position could be accomplished by movement of the C6-phosphate while the C1-phosphate binding site remains the same.

Both the structural evidence and the kinetics of the mutant aldolases are consistent with the existence of two alternative C6-phosphate binding subsites. Movement between subsites is achieved by repositioning the Fru-1,6-P_2 as found in the K146A·Fru-1,6-P_2 structure toward Lys-107, placing the C-2 carbonyl in position for nucleophilic attack by Lys-229. Arg-148, rather than acting as a C1-phosphate ligand (*59*),

remains in an ion-pair with Glu-189, and the methylene groups of this side chain lie along one wall of the active-site cleft (Figure 1) in which the substrate travels by moving between subsites. Furthermore, as mentioned above, this movement of the substrate might trigger the movement of the C-terminus by release of Arg-303−substrate binding and subsequent interaction of the guanidino group with Glu-354, a conserved residue in all aldolase A enzymes. This is consistent with the effects on k_{cat} in the R303A mutant with both Fru-1,6-P_2 and Fru-1-P.

This structure raises a number of questions, such as how the substrate moves between subsites on the enzyme and what role the C-terminus plays, if any. Future studies will involve trapping the substrate bound to the subsite for covalent catalysis by using inhibitors, cocrystallization, and/or reduction of the hexose−Schiff base with sodium borohydride and subsequent crystallization. Previous attempts at crystallization of the borohydride-reduced enzyme−substrate complex using the wild-type enzyme have been unsuccessful, possibly due to the heterogeneity produced by the existence of a combination of hexose− and DHAP−Schiff base enzyme forms (*69*). K146A, which does not go on to form the DHAP−Schiff base, would be ideal for these experiments.

ACKNOWLEDGMENT

We thank Michael Rynkewitz for his assistance in data collection.

REFERENCES

1. Rutter, W. J. (1964) *Fed. Proc. 23*, 1248−1257.
2. Tolan, D. R., Niclas, J., Bruce, B. D., and Lebo, R. V. (1987) *Am. J. Hum. Genet. 41*, 907−924.
3. Penhoet, E. E., Kochman, M., Valentine, R., and Rutter, W. J. (1967) *Biochemistry 6*, 2940−2949.
4. Creighton, D. J., and Murthy, N. S. R. K. (1990) *Enzymes (3rd Ed.) 19*, 323−421.
5. Penhoet, E. E., Rajkuman, R., and Rutter, W. J. (1966) *Proc. Natl. Acad. Sci. U.S.A. 56*, 1275−1282.
6. Penhoet, E. E., Kochman, M., and Rutter, W. J. (1969) *Biochemistry 8*, 4396−4402.
7. Matsushima, T., Kawabe, S., Shibuya, M., and Sugimura, T. (1968) *Biochem. Biophys. Res. Commun. 30*, 565−570.
8. Steinmann, B., and Gitzelmann, R. (1981) *Helv. Paediat. Acta 36*, 297−316.
9. Tolan, D. R. (1995) *Hum. Mutat. 6*, 210−218.
10. Dalby, A., and Littlechild, J. A. (1996) *J. Pharm. Pharmacol. 48*, 214−217.
11. Kim, H., Certa, U., Dobeli, H., Jakob, P., and Hol, W. G. (1998) *Biochemistry 37*, 4388−4396.
12. Rose, I. A., Warms, J. V. B., and Kuo, D. J. (1987) *J. Biol. Chem. 262*, 692−701.
13. Allen, K. N. (1998) in *Comprehensive Biological Catalysis* (Sinnott, M., Ed.) pp 135−172, Academic Press, New York.
14. Lai, C. Y., and Oshima, T. (1971) *Arch. Biochem. Biophys. 144*, 363−374.
15. Littlechild, J., and Watson, H. (1993) *Trends Biochem. Sci. 18*, 36−39.
16. Sygusch, J., Beaudry, D., and Allaire, M. (1987) *Proc. Natl. Acad. Sci. U.S.A. 84*, 7846−7850.
17. Morris, A. J., and Tolan, D. R. (1994) *Biochemistry 33*, 12291−12297.
18. Gamblin, S. J., Davies, G. J., Grimes, J. M., Jackson, R. M., Littlechild, J. A., and Watson, H. C. (1991) *J. Mol. Biol. 219*, 573−576.
19. Hester, G., Brenner-Holzach, O., Rossi, F. A., Struck, D. M., Winterhalter, K. H., Smit, J. D., and Piontek, K. (1991) *FEBS Lett. 292*, 237−242.
20. Blom, N., and Sygusch, J. (1997) *Nat. Struct. Biol. 4*, 36−39.
21. Morris, A. J., and Tolan, D. R. (1993) *J. Biol. Chem. 268*, 1095−1100.
22. Morris, A. J., Davenport, R. C., and Tolan, D. R. (1996) *Protein Eng. 9*, 61−67.
23. Blonski, C., De Moissac, D., Perie, J., and Sygusch, J. (1997) *Biochem. J. 323*, 71−77.
24. Hartman, F. C., and Barker, R. (1965) *Biochemistry 4*, 1068−1075.
25. Sygusch, J., and Beaudry, D. (1984) *J. Biol. Chem. 259*, 10222−10227.
26. Dalby, A., Dauter, Z., and Littlechild, J. A. (1999) *Protein Sci. 8*, 291−297.
27. Sanger, F., Nicklen, S., and Coulson, A. R. (1977) *Proc. Natl. Acad. Sci. U.S.A. 74*, 5463−5487.
28. Barr, P. J., Thayer, R., Laybourne, P., Najarian, R. C., Seela, F., and Tolan, D. R. (1986) *Bio/Technology 4*, 428−432.
29. Laemmli, U. K. (1970) *Nature 227*, 680−686.
30. Baranowski, T., and Niederland, T. R. (1949) *J. Biol. Chem. 180*, 543−551.
31. Racker, E. (1952) *J. Biol. Chem. 196*, 347−351.
32. Cleland, W. W. (1990) *Enzymes (3rd Ed.) 19*, 99−158.
33. Otwinowski, Z., and Minor, W. (1997) *Methods Enzymol. 276*, 307−326.
34. Navaza, J. (1994) *Acta Crystallogr. A50*, 157−163.
35. CollaborativeComputationalProjectNumber4 (1994) *Acta Crystallogr. D50*, 760−763.
36. Matthews, B. W. (1985) *Methods Enzymol. 114*, 176−187.
37. Tong, L., and Rossmann, M. G. (1990) *Acta Crystallogr. A46*, 783−792.
38. Brünger, A. T. (1992) *Nature 355*, 472−474.
39. Brünger, A. T. (1992) *X-PLOR, Version 3.1 A system for X-ray crystallography and NMR*, Yale University Press, New Haven.
40. Jones, T. A., Zou, J. Y., Cowan, S. W., and Kjeldgaard, M. (1991) *Acta Crystallogr. A47*, 110−119.
41. Jones, T. A. (1992) in *Molecular Replacement* (Dodson, E. J., Gover, S., and Wolf, W., Eds.) pp 91−105, SERC Daresbury Laboratory, Warrington.
42. Tolan, D. R., Amsden, A. B., Putney, S. D., Urdea, M. S., and Penhoet, E. E. (1984) *J. Biol. Chem. 259*, 1127−1131.
43. Lai, C. Y., Nakai, N., and Chang, D. (1974) *Science 183*, 1204−1206.
44. Laskowski, R. A., MacArthur, M. W., Moss, D. S., and Thornton, J. M. (1993) *J. Appl. Crystallogr. 26*, 283−291.
45. Hartman, F. C., and Welch, M. H. (1974) *Biochem. Biophys. Res. Commun. 57*, 85−92.
46. Dreschler, E. R., Boyer, P. D., and Kowalsky, A. G. (1959) *J. Biol. Chem. 234*, 2627−2634.
47. Spolter, P. D., Adelman, R. C., and Weinhouse, S. (1965) *J. Biol. Chem. 240*, 1327−1337.
48. Rose, I. A., and O'Connell, E. L. (1969) *J. Biol. Chem. 244*, 126−134.
49. Berthiaume, L., Loisel, T. P., and Sygusch, J. (1991) *J. Biol. Chem. 266*, 17099−17105.
50. Berthiaume, L., Tolan, D. R., and Sygusch, J. (1993) *J. Biol. Chem. 268*, 10826−10835.
51. Berardini, T. Z., Drygas, W. M., Callard, G. V., and Tolan, D. R. (1997) *Comp. Biochem. Physiol. 117*, 471−476.
52. Berardini, T., Amsden, A. B., Penhoet, E. E., and Tolan, D. R. (1999) *Comp. Biochem. Physiol. 122*, 53−61.
53. Grazi, E., and Trombetta, G. (1987) *Int. J. Biochem. 19*, 197−200.
54. Grazi, E., and Trombetta, G. (1984) *Arch. Biochem. Biophys. 233*, 595−602.
55. Grazi, E., Trombetta, G., and Lanzara, V. (1983) *Biochem. Biophys. Res. Commun. 110*, 578−583.
56. Blonski, C., Gefflaut, T., and Perie, J. (1995) *Bioorg. Med. Chem. 3*, 1247−1253.
57. Gefflaut, T., Blonski, C., Perie, J., and Willson, M. (1995) *Prog. Biophys. Mol. Biol. 63*, 301−340.

58. Lewis, D. J., and Lowe, G. (1977) *Eur. J. Biochem. 80*, 119−133.
59. Lobb, R. R., Stokes, A. M., Hill, H. A., and Riordan, J. F. (1976) *Eur. J. Biochem. 70*, 517−522.
60. Anai, M., Lai, C. Y., and Horecker, B. L. (1973) *Arch. Biochem. Biophys. 156*, 712−719.
61. Wang, J., Morris, A. J., Tolan, D. R., and Pagliaro, L. (1996) *J. Biol. Chem. 271*, 6861−6865.
62. Gamblin, S. J., Cooper, B., Millar, J. R., Davies, G. J., Littlechild, J. A., and Watson, H. C. (1990) *FEBS Lett. 262*, 282−286.
63. Kochman, M., and Dobryszycki, P. (1991) *Acta Biochim. Pol. 38*, 407−421.
64. Baron, C. B., Tolan, D. R., Choi, K. H., and Coburn, R. F. (1999) *Biochem. J. 341*, 805−812.
65. Midelfort, C. F., Gupta, R. K., and Rose, I. A. (1976) *Biochemistry 15*, 2178−2185.
66. Rose, I. A., and O'Connell, E. L. (1977) *J. Biol. Chem. 252*, 479−482.
67. Wurster, B., and Hess, B. (1973) *Biochem. Biophys. Res. Commun. 55*, 985−992.
68. Schray, K. J., Fishbein, R., Bullard, W. P., and Benkovic, S. J. (1975) *J. Biol. Chem. 250*, 4883−4887.
69. DiIasio, A., Trombetta, G., and Grazi, E. (1977) *FEBS Lett. 73*, 244−246.
70. Kraulis, P. J. (1991) *J. Appl. Crystallogr. 24*, 946−950.
71. Nicholls, A., Sharp, K., and Honig, B. (1991) *Proteins: Struct., Funct., Genet. 11*, 281−296.

BI9828371